

A compact permanent-magnet system for measuring magnetic circular dichroism in resonant inelastic soft X-ray scattering

Jun Miyawaki,^{a,b*} Shigemasa Suga,^c Hidenori Fujiwara,^d Hideharu Niwa,^{a,b,‡} Hisao Kiuchi^{e,§} and Yoshihisa Harada^{a,b}

Received 13 October 2016

Accepted 18 January 2017

Edited by M. Yamamoto, RIKEN SPring-8 Center, Japan

‡ Present address: Division of Physics, Faculty of Pure and Applied Sciences, University of Tsukuba, Tsukuba, Ibaraki 305-8571, Japan.

§ Present address: Office of Society-Academia Collaboration for Innovation, Kyoto University, Gokasho, Uji, Kyoto 611-0011, Japan.

Keywords: soft X-ray RIXS; magnetic circular dichroism; Nd–Fe–B permanent magnet; sample transfer system.

^aThe Institute for Solid State Physics, The University of Tokyo, Kashiwanoha, Kashiwa, Chiba 277-8581, Japan,

^bSynchrotron Radiation Research Organization, The University of Tokyo, Hongo, Bunkyo-ku, Tokyo 113-8656, Japan,

^cInstitute of Scientific and Industrial Research, Osaka University, Ibaraki, Osaka 567-0047, Japan, ^dDivision of Materials Physics, Graduate School of Engineering Science, Osaka University, Toyonaka, Osaka 560-8531, Japan, and

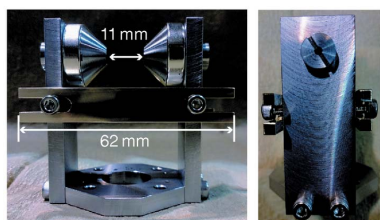
^eDepartment of Applied Chemistry, The University of Tokyo, Hongo, Bunkyo-ku, Tokyo 113-8656, Japan.

*Correspondence e-mail: miyawaki@issp.u-tokyo.ac.jp

A compact and portable magnet system for measuring magnetic dichroism in resonant inelastic soft X-ray scattering (SX-RIXS) has been developed at the beamline BL07LSU in SPring-8. A magnetic circuit composed of Nd–Fe–B permanent magnets, which realised ~ 0.25 T at the center of an 11 mm gap, was rotatable around the axis perpendicular to the X-ray scattering plane. Using the system, a SX-RIXS spectrum was obtained under the application of the magnetic field at an angle parallel, nearly 45° or perpendicular to the incident X-rays. A dedicated sample stage was also designed to be as compact as possible, making it possible to perform SX-RIXS measurements at arbitrary incident angles by rotating the sample stage in the gap between the magnetic poles. This system enables facile studies of magnetic dichroism in SX-RIXS for various experimental geometries of the sample and the magnetic field. A brief demonstration of the application is presented.

1. Introduction

Resonant inelastic X-ray scattering (RIXS), especially soft X-ray RIXS (SX-RIXS), has made remarkable progress in terms of energy resolution over the past few decades in conjunction with the improvement of the performance of synchrotron radiation sources and advancements in the RIXS instrumentation. Accordingly, RIXS has come to occupy an important position in X-ray spectroscopy techniques for investigating the bulk electronic structures (Kotani & Shin, 2001; Ament *et al.*, 2011). One of the major scientific motivations for pursuing the development of SX-RIXS is that the SX region covers important absorption edges such as the *K*-edges of light elements (C, N and O) and the *L*-edges of 3*d* transition metals. Therefore, SX-RIXS is very suitable for investigating the electronic structures of strongly correlated transition metal oxides, which exhibit various electrical properties as represented by high-temperature copper-oxide-based superconductors as well as a wide variety of magnetic properties ranging from ferromagnetism to antiferromagnetism. Another research motivation is that the improvement in the energy resolution in SX-RIXS has allowed access to elementary excitations such as *dd* excitations, orbitons, magnons and phonons, which determine important physical properties such as electric transport and magnetism. Thus, SX-RIXS has made a significant contribu-



tion to the comprehension of many-body physics in strongly correlated materials, especially transition metal oxides. RIXS has also been applied to many materials regardless of their states of matter (solid, liquid and gas) as well as electrical conductivity (metallic, semiconducting or insulating). This photon-in/photon-out RIXS experiment has many advantages, such as bulk sensitivity; element-, orbital- and chemical-selectivity; and energy-, momentum- and polarization-dependence. Additionally, the photon-in/photon-out process adds to RIXS the distinctive feature that the electronic structure can be measured even in an electronic and/or magnetic field. Regarding the use of the magnetic field for RIXS, magnetic circular dichroism (MCD) in RIXS (RIXS-MCD) has intensively been used to extract spin-resolved valence band excitations (Duda, 2000; Braicovich *et al.*, 2001; Braicovich, 2005).

RIXS-MCD was first theoretically predicted by Strange *et al.* (1991). It principally provides information similar to that obtained from spin-resolved photoemission spectroscopy, and is complementary to MCD in X-ray absorption spectroscopy (XAS) (*i.e.* XMCD). Experimentally, Duda *et al.* conducted the first work on MCD in the X-ray fluorescence from 3d itinerant magnets (Duda *et al.*, 1994), followed by the measurement of RIXS-MCD for localized magnets (Yablonskikh *et al.*, 2001). Braicovich *et al.* advanced RIXS-MCD on the condition that XMCD was not obtained using the so-called 'forbidden' geometry, where the magnetization of the sample was perpendicular to the helicity vector of the circularly polarized X-rays (Braicovich *et al.*, 1999). This condition gives the advantage of suppressing the polarization-dependent self-absorption effect of the scattered X-rays resulting from the different penetration depth owing to XMCD (Braicovich *et al.*, 1998). Then, RIXS-MCD is induced by the different probability of the relaxation to the polarized core-hole created by the resonant excitation using left- and right-circularly polarized X-rays (van der Laan & Thole, 1995; van der Laan, 2015). Thus, bulk ground-state magnetic moments that are impossible to observe by conventional XMCD and spin-resolved photoemission spectroscopy can be obtained. In spite of tremendous efforts made so far by many researchers, RIXS-MCD is far from being a commonly used technique, which is in contrast to XMCD. One reason for this is the difficulties in the RIXS experiment compared with XAS. Another and more fundamental reason is that a quantitative and reliable theoretical analysis is required for RIXS-MCD, which has not yet been established. This situation contrasts sharply with XMCD, wherein sum rules have been established by Thole *et al.* (Thole *et al.*, 1992; Carra *et al.*, 1993) that have made XMCD a strong quantitative analysis technique for magnetic moments.

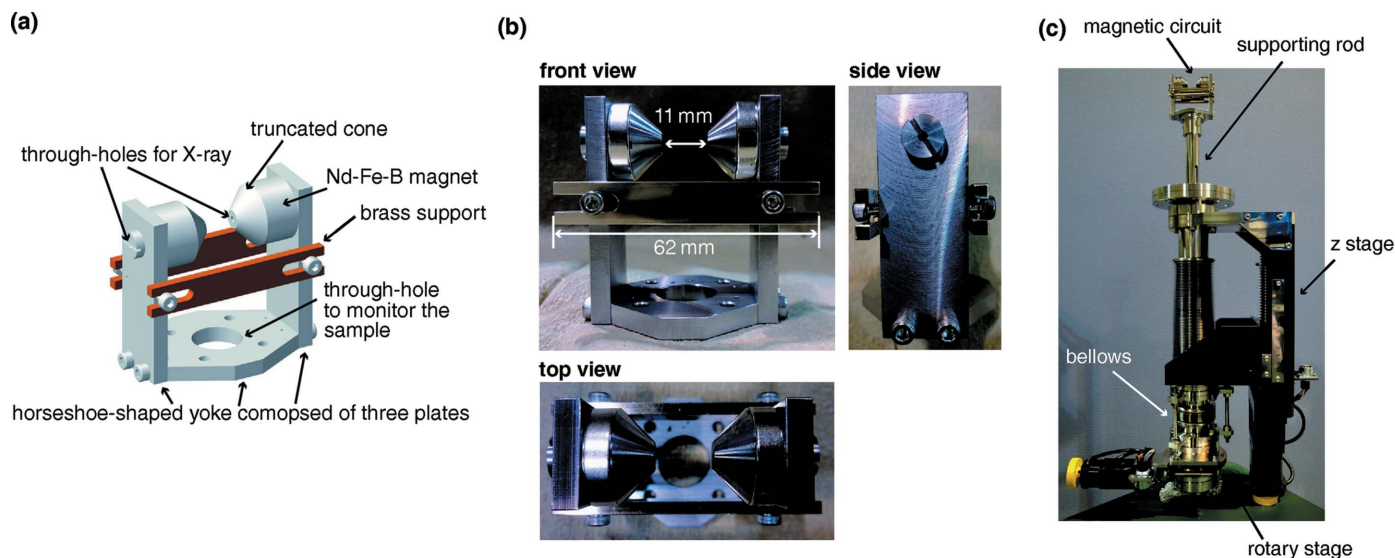
However, the potential of the RIXS-MCD technique more than compensates for the lack of sum rules. In addition to all the features inherited from RIXS itself, RIXS-MCD of *dd* excitations that can easily be separated by the use of the latest high-energy-resolution RIXS apparatus can provide magnetic information for each localized *d* orbital. With these advantages, RIXS-MCD is becoming a very promising technique, and is expected to be successfully applied to new functional

materials in which spin plays important roles, such as multiferroics and those to be used for spintronic devices. In order to demonstrate the significance of RIXS-MCD with high energy resolution and encourage its wider use, it is highly desired that RIXS-MCD experiments can be performed as a common tool at any RIXS end-station in worldwide synchrotron radiation facilities. Therefore, we have developed a compact and portable magnet system for RIXS-MCD composed of Nd-Fe-B permanent magnets which can generate a magnetic field of ~ 0.25 T. Although electromagnets or superconducting magnets can be used for the source of the stronger magnetic field, permanent magnets were chosen to increase the portability and flexibility of the measuring system. For the transition metal oxides intensively studied by RIXS, the magnetic fields produced by the permanent magnets were strong enough to obtain the single magnetic domain necessary for RIXS-MCD measurements. This is because most transition metal oxides are soft magnets, and their coercive fields are relatively small. In this paper, we describe the design of the developed magnet system and the function of the individual components, and finally report some results of RIXS-MCD measured by this system.

2. Design and construction

Figs. 1(a) and 1(b) display a schematic drawing and photographs of the originally designed magnetic circuit. The magnetic circuit consists of Nd-Fe-B magnets, a horseshoe-shaped yoke, truncated cone poles and two supports. The Nd-Fe-B magnets are the source of the magnetic field. The horseshoe-shaped yoke and truncated cone poles are made of Fe, and functions to focus the magnetic fields. The two supports are made of brass, and function to resist the attractive force between the magnets. The overall size of the magnetic circuit is within 65 mm-diameter so that it can be installed through and mounted on the most commonly used 4-1/2 inch-diameter ConFlat[®] flange. This compact design of the magnetic circuit allows it to be installed without any modification to the existing vacuum chambers and optical systems for RIXS. Additionally, the length of the gap between the magnetic poles can be varied by exchanging the components with those of different sizes for the magnetic circuit, whereby existing sample stages of various sizes can be accommodated. Through-holes shown in Figs. 1(a) and 1(b) are used as follows. The through-hole in the bottom plate is used to monitor the relative position of the sample between the magnetic poles. The 2 mm-diameter through-holes in the magnetic poles are used to allow the X-ray beam to pass through.

Fig. 1(c) shows a photograph of a magnet system composed of the magnetic circuit and positioning mechanisms including *z*-stage, rotary stage and bellows for angle adjustment. The *z*-stage is used to move the magnetic circuit linearly to the sample position, and also enables retraction of the circuit in order to carry out a normal RIXS experiment without a magnetic field. The rotary stage provides the rotary motion of the magnetic circuit, and allows measurements to determine the dependence upon the direction of the magnetization and

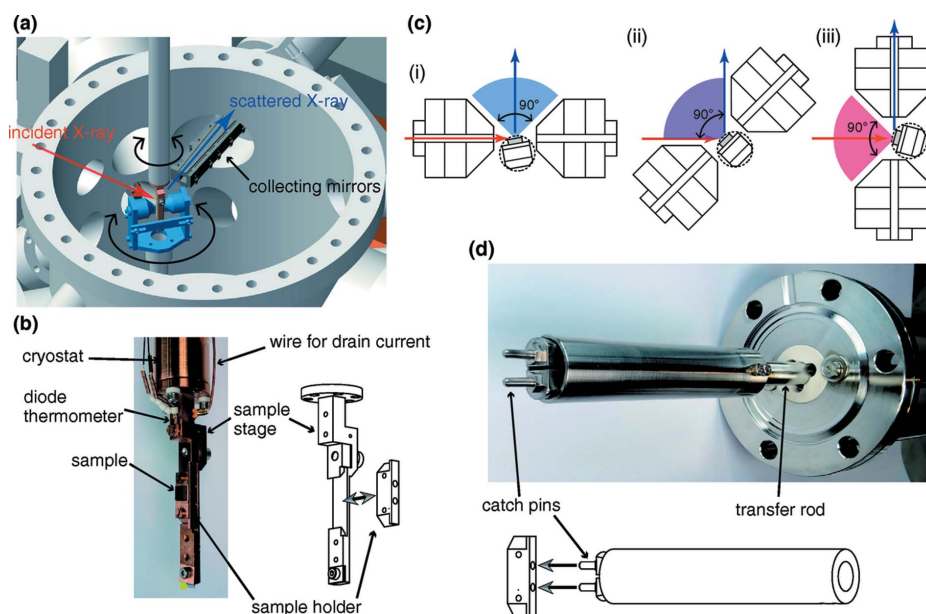

Figure 1

Schematic representation and photographs of the magnet system. (a) Schematic representation and (b) photographs of the magnetic circuit. The magnetic circuit is composed of Nd–Fe–B magnets, a horseshoe-shaped yoke and truncated cones made of Fe, and brass supports. The magnets are fixed by a screw with a through-hole for the X-ray beam. (c) Photograph of the complete magnet system.

to obtain MCD by reversing the magnetization. The supporting rod for the magnetic circuit is a hollow pipe. This ensures that a sample located between the magnetic poles can be monitored from the bottom port through the hole in the bottom plate of the yoke, facilitating sample position adjustment. The strength of the magnetic fields depends upon the dimensions of the magnetic circuit, particularly the length of the gap between the magnetic poles. At a gap of 11 mm, which is the optimized gap size for a particularly dedicated sample stage described later, the magnetic field of the magnetic circuit was measured to be ~ 0.25 T at the center of the poles.

Fig. 2(a) shows a schematic representation of the experimental configuration in a vacuum chamber using this magnet system at the HORNET end-station in SPring-8 BL07LSU (Harada *et al.*, 2012; Yamamoto *et al.*, 2014). The magnet system and sample stage were installed from the bottom and top of the vacuum chamber, respectively, and the scattering angle was fixed at 90° . A dedicated sample stage for the magnet system is shown in Fig. 2(b). This sample stage was designed to accommodate one sample holder, which was tightly attached to the stage by fastening a screw bolt behind to obtain good electrical contact and thermal conductivity. The sample stage was fixed to a cryostat to control the sample temperature

between 30 and 500 K. The sample stage is electrically insulated from the cryostat by a sapphire plate between the stage and the cryostat, which enables the XAS to be measured in total electron yield (TEY) mode by measuring the drain current. The experimental parameters for the RIXS-MCD experiment are summarized in Table 1.


Figure 2

Schematic representation and photographs of the experimental setup and the dedicated sample transfer system. (a) Experimental configuration of RIXS-MCD at the HORNET end-station in SPring-8 BL07LSU when the angle of the magnetic field is set at 45° to the incident X-ray. (b) Sample stage fixed to a cryostat with a mounted sample. (c) Cross-sectional views of the experimental configurations of RIXS-MCD on the scattering plane. The red and blue arrows indicate the incident and scattered X-rays, respectively. The colored quadrants represent the clearance angle for the incident and/or scattered X-rays. The 9 mm-diameter dotted circle around the sample stage indicates the area required for rotating the sample stage with a mounted sample. (d) Catching device for the transfer of the sample mounted on the end of a transfer rod.

Table 1

Experimental parameters for the RIXS-MCD experiment at the HORNET end-station in SPring-8 BL07LSU (Harada *et al.*, 2012; Yamamoto *et al.*, 2014).

BL07LSU in SPring-8	
Energy range of beamline	250–2000 eV
Photon flux	$>10^{12}$ photons s^{-1}
Energy resolution of beamline	$E/\Delta E > 10000$
Polarization	Linear (horizontal, vertical and variable angles of the polarization plane) Circular (left, right and elliptical)
HORNET end-station	
Spot size	$\sim 5 \mu\text{m}$ (V) $\times \sim 30 \mu\text{m}$ (H)
Energy range of spectrometer	350–750 eV
Energy resolution of spectrometer	$E/\Delta E \geq 8000$ in the range 350–550 eV $E/\Delta E \geq 6400$ in the range 550–750 eV
Magnitude of magnetic field	~ 0.25 T
Vacuum pressure	$\sim 2 \times 10^{-6}$ Pa without baking
Sample transfer	Available
Sample size	$< 7 \text{ mm} \times 16 \text{ mm}$
Sample temperature	30–500 K
XAS by TEY	Available by the drain current from sample
XAS by PFY	Available by the silicon drift detector

Fig. 2(c) illustrates the cross-sectional views on the scattering plane for the experimental configurations. The width of the sample stage and the gap between the magnetic poles were set to be 7 and 11 mm, respectively. The through-holes in the magnetic poles can be used for the incident or scattered X-rays. Since the through-holes are bored in both magnetic poles, the magnetic field reversal is allowed by the 180° rotation of the magnetic circuit. The clearance angle for the X-rays is larger than 90°, as indicated by the colored quadrants in Fig. 2(c). Thus, in the case of the fixed scattering angle of 90°, the three configurations are available. The magnet system can be set at one of the fixed angles of (i) parallel, (ii) $\sim 45^\circ$ and (iii) perpendicular to the incident X-ray, as shown in Fig. 2(c). In the configurations of (i) and (ii), the scattered X-rays are not blocked by the magnet system. Therefore, RIXS-MCD can be measured with the collecting mirrors in the configurations of (i) and (ii). However, in the configuration of (iii), the acceptance angle for the scattered X-rays is limited to $\sim 3.5^\circ$ by the 2 mm-diameter through-hole. The horizontal and vertical acceptance angles for the RIXS spectrometer at the HORNET end-station are $\sim 0.6^\circ$ and $\sim 0.3^\circ$, respectively. Thus, RIXS-MCD can be measured in the configuration (iii), though the collecting mirrors are not available. For the q -dependent RIXS, the large clearance angle allows us to change the angle of the scattered [incident] X-rays in the configuration (i) [(iii)]. In the configuration of (ii), the incident and/or scattered X-rays can be changed. The overall size of the sample stage including the sample holder and sample is within 9 mm-diameter, which is indicated by the dotted circle in Fig. 2(c). Thus, the sample stage can be rotated in the magnetic circuit of the 11 mm gap between the magnetic poles, and the X-rays can be irradiated on the sample with an arbitrary incident angle.

Fig. 2(d) shows the sample catching device used for the transfer of the sample holder to the sample stage. To securely catch a small sample holder with 7 mm width and 3.5 mm

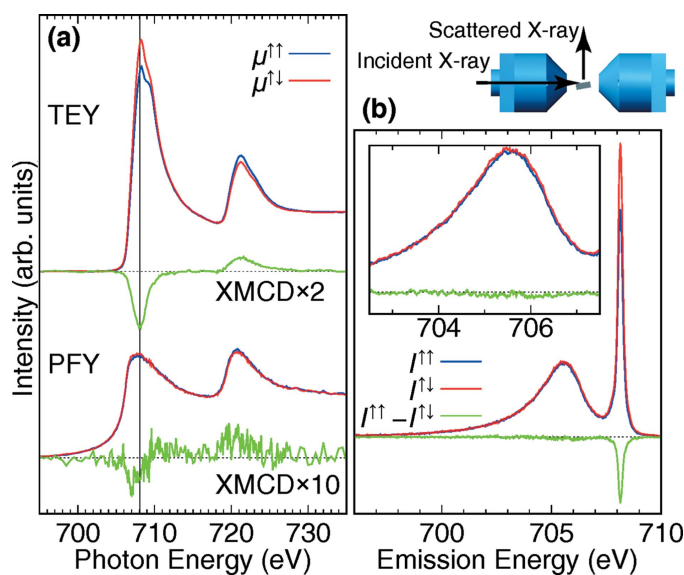
thickness, two holes are placed in the sample holder, which match with two catch pins of the catching device mounted on the end of a transfer rod. When a sample is transferred to and from the stage, the catch pins are inserted into the holes, and the subsequent rotation of the transfer rod narrows the gap of the two catch pins. Therefore, the holder is securely gripped.

3. Results of RIXS-MCD measurements

Here we show some examples of the experimental results obtained by the developed magnet system to demonstrate its capability. The scientific aspects of the results will not be discussed in detail, but an emphasis is placed on the experimental setup and practical measurement procedure.

3.1. Fe L -edge RIXS-MCD of Terfenol-D

To confirm the performance of this magnet system, the Fe L -edge XMCD and RIXS-MCD of a Terfenol-D ($\text{Tb}_{0.3}\text{Dy}_{0.7}\text{Fe}_2$) quasi-single-crystal were measured (Clark & Wun-Fogle, 2002). Both XMCD and RIXS-MCD measurements were conducted in the normal XMCD geometry, where the helicity vector of the circularly polarized incident X-rays was parallel to the direction of the magnetization. As schematically shown in Fig. 3, the magnet was placed parallel to the incident X-rays [the configuration of (i) in Fig. 2(c)], and a 10° grazing incidence was adopted to magnetize the sample along the easy magnetization axis on the sample surface. The size of the sample was 5 mm \times 5 mm \times 2 mm (thickness), and the footprint of the X-ray on the sample was $\sim 200 \mu\text{m}$ ($\sim 5 \mu\text{m}$) along (perpendicular to) the direction of the magnetic field. The oxidized surface layers were removed by polishing the sample surface in an Ar atmosphere. The sample was installed in the vacuum chamber without being exposed to the air, and XAS was measured in both TEY and partial fluorescence yield (PFY) modes. To perform XAS measurements by the TEY mode, a negative retarding voltage of 9 V was applied to the sample to avoid the influence from the reabsorption of photoelectrons owing to the magnetic field, which might distort the XAS profile. The PFY XAS spectrum was obtained using a silicon drift detector mounted at 45° from the incident X-rays on the scattering plane. Fig. 3(a) shows the XAS spectra measured by left- and right-circularly polarized X-rays and the XMCD spectra obtained by the difference of these two spectra. In the TEY mode, a shoulder structure was observed because of the surface oxidation. In the PFY mode, however, a featureless single broad peak typical of metallic Fe was obtained, indicating that the thickness of the oxidized surface layers was less than several atomic layers. In the TEY mode, XMCD signal was mainly observed at the peak of the Fe metal, namely around $h\nu = 708.1$ eV. The values of the asymmetry $[(\mu^{\uparrow\uparrow} - \mu^{\uparrow\downarrow})/(\mu^{\uparrow\uparrow} + \mu^{\uparrow\downarrow})]$ at the L_3 - and L_2 -edges were approximately -6.5 and 2.8% , respectively, which agree very well with a previous report (Arenholz & Prestemon, 2004). In the PFY mode, however, XMCD was very small due to the self-absorption effect, but the trend is rather similar to that seen in the TEY mode.


Figure 3

Fe L -edge XMCD and RIXS-MCD spectra of a Terfenol-D ($\text{Tb}_{0.3}\text{Dy}_{0.7}\text{Fe}_2$) quasi-single-crystal. A sketch of the experimental configuration is also presented in the upper right. (a) Fe $L_{2,3}$ -edge XAS spectra measured in TEY and PFY mode together with their XMCD spectra. The blue ($\mu^{\uparrow\uparrow}$) and red ($\mu^{\uparrow\downarrow}$) spectra represent the absorption intensity for the helicity of the circularly polarized incident X-rays parallel and antiparallel to the macroscopic magnetization, respectively. To show XMCD, the difference spectra ($\mu^{\uparrow\uparrow} - \mu^{\uparrow\downarrow}$) are multiplied by 2 and 10 for TEY and PFY, respectively, and plotted by green lines. (b) The circular-polarization dependence of RIXS spectra measured at $h\nu = 708.1$ eV indicated by a vertical line in (a). The blue ($I^{\uparrow\uparrow}$) and red ($I^{\uparrow\downarrow}$) spectra represent the RIXS intensity for the helicity of the circularly polarized incident X-rays parallel and antiparallel to the macroscopic magnetization, respectively. The difference spectrum ($I^{\uparrow\uparrow} - I^{\uparrow\downarrow}$) is plotted by a green line. (Inset) Enlarged plot of the peaks at ~ 705.5 eV.

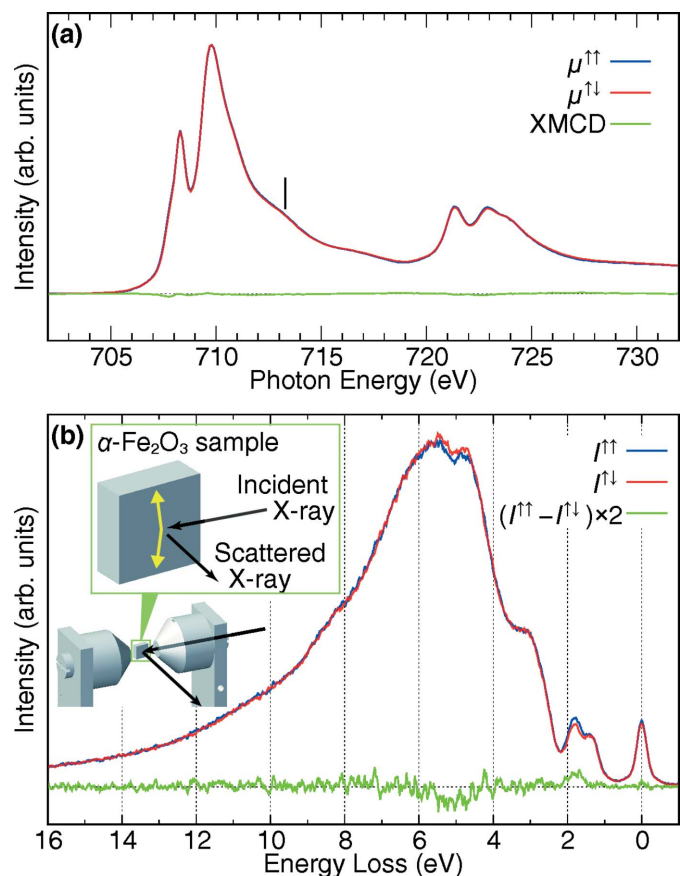
Fig. 3(b) shows the circular-polarization dependence of RIXS spectra excited at $h\nu = 708.1$ eV. Although the sharp elastic peak at $h\nu = 708.1$ eV and the broad fluorescent peak around $h\nu = 705.5$ eV were well separated, no elementary excitation was observed. This result also indicates the metallic nature of the sample. The RIXS-MCD spectrum is dominated by the elastic peak, but the difference at the fluorescent peak is almost absent. This result is associated with similar observations in Mn alloys (Duda, 2000; Yablonskikh *et al.*, 2001), implying that there exists the contribution from localized magnetic moments. Thus, RIXS-MCD gives useful information which is complementary to XMCD.

3.2. Fe L -edge RIXS-MCD of $\alpha\text{-Fe}_2\text{O}_3$

To demonstrate that the ability of RIXS-MCD is greater than that of XMCD, the Fe L -edge RIXS-MCD of $\alpha\text{-Fe}_2\text{O}_3$ was measured. An $\alpha\text{-Fe}_2\text{O}_3(111)$ single crystal of size $5\text{ mm} \times 5\text{ mm} \times 2\text{ mm}$ (thickness) was used. The crystal sample had a mirror-polished surface, and was installed in the vacuum chamber without any surface treatment. The exchange coupling of $\alpha\text{-Fe}_2\text{O}_3$ is essentially antiferromagnetic. However, $\alpha\text{-Fe}_2\text{O}_3$ shows weak ferromagnetism due to Dzyaloshinskii–Moriya interaction at room temperature (Dzyaloshinsky, 1958; Moriya, 1960). In the weak ferromagnetic phase, the spin

magnetic moments of $\alpha\text{-Fe}_2\text{O}_3$ are on the (111) plane. Thus, the weak ferromagnetic nature of this compound allows us to obtain a single magnetic domain by applying a magnetic field along the (111) plane (Martin-Hernandez & Guerrero-Suárez, 2012). For both XMCD and RIXS-MCD experiments, the same experimental configuration as that for Terfenol-D was used. The magnet was placed parallel to the incident X-ray [configuration (i) in Fig. 2(c)], and a 10° grazing incidence was adopted. In this configuration, the weak ferromagnetic moments are aligned on the (111) plane by the surface-parallel component of the magnetic field, as schematically shown in Fig. 4(b). Then, the dominant antiferromagnetic moments become perpendicular to the magnetic field as well as the incident X-rays.

Fig. 4(a) shows the XAS spectra measured by circularly polarized X-rays in the TEY mode and the XMCD spectrum. No discernible signal was detected in its XMCD spectrum. This was because the net magnetic moment owing to the weak


Figure 4

Fe L -edge XMCD and RIXS-MCD spectra of an $\alpha\text{-Fe}_2\text{O}_3(111)$ single crystal. (a) Fe $L_{2,3}$ -edge XAS spectra measured by circularly polarized X-rays in TEY mode together with the XMCD spectrum. (b) RIXS-MCD spectra measured at $h\nu = 713.25$ eV indicated by a vertical line in (a). To clearly show RIXS-MCD, the difference spectrum ($I^{\uparrow\uparrow} - I^{\uparrow\downarrow}$) is multiplied by 2, and plotted by a green line in the same graph. A sketch of the experimental configuration with the orientation of the spin is shown in the inset. The magnetic field is parallel to the incident X-rays and the incident angle is 10° from the sample surface. Yellow arrows on the $\alpha\text{-Fe}_2\text{O}_3(111)$ sample represent the direction of the antiferromagnetically coupled and canted spin moments on the (111) plane.

ferromagnetism was too small to be detected. Fig. 4(b) exhibits the RIXS-MCD spectra measured at a photon energy of 713.25 eV which corresponds to the absorption energy of the charge-transfer satellite as indicated by the solid line in Fig. 4(a) (Kuiper *et al.*, 1993; de Groot *et al.*, 2005). The circular-polarization dependence was clearly observed at 1.8 and 4.85 eV loss energies, and this dichroism was the RIXS-MCD signal since the sign of the dichroism was reversed by the reversal of the direction of the magnetization. The peaks at the loss energies of 1.8 and 4.85 eV are assigned to a *dd* excitation from ${}^6A_{1g}$ to ${}^4T_{2g}$ and to a charge-transfer transition, respectively (Marusak *et al.*, 1980). Accordingly, RIXS-MCD was clearly observed by high-energy-resolution RIXS, though XMCD was not observed. These results confirmed that the observed RIXS-MCD was induced by the RIXS process, *via* the relaxation of valence electrons to polarized core-holes created by the circularly polarized X-rays. Thus, the application of RIXS-MCD to α -Fe₂O₃ demonstrates that more useful bulk information about the ground-state spin state can be obtained by using RIXS-MCD than by using XMCD.

4. Summary and outlook

A compact and portable magnet system for RIXS-MCD was developed at the HORNET end-station in SPring-8 BL07LSU with a dedicated sample stage and sample transfer system. The magnetic circuit worked as designed, and generated a magnetic field of ~ 0.25 T. Using this system, XMCD and RIXS-MCD were successfully acquired by the reversal of the magnetic field. The capability of the magnet system was demonstrated by RIXS-MCD measurements, and the advantage was clearly shown by the RIXS-MCD measurement of a weak ferromagnetic α -Fe₂O₃ sample. In antiferromagnets, XMCD signal cannot be principally obtained, and X-ray magnetic linear dichroism generally provides information about the direction of the magnetization. In contrast, RIXS-MCD can be applied also to antiferromagnets, and can shed light on the bulk ground-state magnetic moments. Furthermore, direct information about the magnetic coupling can be revealed by the observation of magnetic field dependence of magnons by *q*-dependent RIXS.

Thus, this compact permanent-magnet system was successfully used for RIXS-MCD, and there are a lot of samples for which the RIXS-MCD is desired to be applied. However, the magnetic field of ~ 0.25 T limits the magnetic materials that can be investigated. In order to align the magnetic moments along the hard magnetization axis, a magnetic field of several Teslas or more is required. However, a large space required for the superconducting magnet makes it difficult to coexist with the optical system for the RIXS spectrometer and the wide scattering angle. We are currently exploring the possibilities of installing a superconducting magnet that has a space-saving design, and is compatible with the wide-scattering-angle experiments. The capability of applying the magnetic field at variable angles is planned to be implemented, which is more suitable for the *q*-dependent RIXS

than the magnetic field at the fixed angle. In addition, for more challenging experiments such as studying the weak magnetization in paramagnets and the magnetoelectronic effect in the multiferroics, a lower temperature sample environment is also needed. We are currently designing a new cryostat that can achieve lower temperature and provide an azimuthal rotation. Combined with a superconducting magnet, RIXS experiments under extreme conditions of high magnetic field and very low temperature are under consideration in our laboratory.

Acknowledgements

This work was carried out by joint research at the Synchrotron Radiation Research Organization and the Institute for Solid State Physics, The University of Tokyo (Proposal Nos. 2014B7474, 2015A7489 and 2015B7497).

References

- Ament, L. J. P., van Veenendaal, M., Devereaux, T. P., Hill, J. P. & van den Brink, J. (2011). *Rev. Mod. Phys.* **83**, 705–767.
- Arenholz, E. & Prestemon, S. O. (2004). *AIP Conf. Proc.* **705**, 1170–1173.
- Braicovich, L. (2005). *J. Electron Spectrosc. Relat. Phenom.* **144–147**, 695–699.
- Braicovich, L., Borgatti, F., Tagliaferri, A., Ghiringhelli, G., Brookes, N., Ferriani, P. & Bertoni, C. (2001). *Appl. Phys. Mater. Sci. Process.* **73**, 679–686.
- Braicovich, L., Dallera, C., Ghiringhelli, G., Brookes, N. & Goedkoop, J. (1998). *Solid State Commun.* **105**, 263–267.
- Braicovich, L., van der Laan, G., Ghiringhelli, G., Tagliaferri, A., van Veenendaal, M. A., Brookes, N. B., Chervinskii, M. M., Dallera, C., De Michelis, B. & Dürr, H. A. (1999). *Phys. Rev. Lett.* **82**, 1566–1569.
- Carra, P., Thole, B. T., Altarelli, M. & Wang, X. (1993). *Phys. Rev. Lett.* **70**, 694–697.
- Clark, A. E. & Wun-Fogle, M. (2002). *Proc. SPIE*, **4699**, 421–436.
- Duda, L.-C. (2000). *J. Electron Spectrosc. Relat. Phenom.* **110–111**, 287–304.
- Duda, L.-C., Stöhr, J., Mancini, D. C., Nilsson, A., Wassdahl, N., Nordgren, J. & Samant, M. G. (1994). *Phys. Rev. B*, **50**, 16758–16761.
- Dzyaloshinsky, I. (1958). *J. Phys. Chem. Solids*, **4**, 241–255.
- Groot, F. M. F. de, Glatzel, P., Bergmann, U., van Aken, P. A., Barrea, R. A., Klemme, S., Hävecker, M., Knop-Gericke, A., Heijboer, W. M. & Weckhuysen, B. M. (2005). *J. Phys. Chem. B*, **109**, 20751–20762.
- Harada, Y., Kobayashi, M., Niwa, H., Senba, Y., Ohashi, H., Tokushima, T., Horikawa, Y., Shin, S. & Oshima, M. (2012). *Rev. Sci. Instrum.* **83**, 013116.
- Kotani, A. & Shin, S. (2001). *Rev. Mod. Phys.* **73**, 203–246.
- Kuiper, P., Searle, B. G., Rudolf, P., Tjeng, L. H. & Chen, C. T. (1993). *Phys. Rev. Lett.* **70**, 1549–1552.
- Laan, G. van der (2015). *J. Electron Spectrosc. Relat. Phenom.* **200**, 143–159.
- Laan, G. van der & Thole, B. T. (1995). *J. Phys. Condens. Matter*, **7**, 9947–9988.
- Martin-Hernandez, F. & Guerrero-Suárez, S. (2012). *Intl J. Earth Sci.* **101**, 637–647.
- Marusak, L., Messier, R. & White, W. B. (1980). *J. Phys. Chem. Solids*, **41**, 981–984.
- Moriya, T. (1960). *Phys. Rev.* **120**, 91–98.
- Strange, P., Durham, P. J. & Gyorffy, B. L. (1991). *Phys. Rev. Lett.* **67**, 3590–3593.

- Thole, B. T., Carra, P., Sette, F. & van der Laan, G. (1992). *Phys. Rev. Lett.* **68**, 1943–1946.
- Yablonskikh, M. V., Yarmoshenko, Y. M., Grebennikov, V. I., Kurmaev, E. Z., Butorin, S. M., Duda, L.-C., Nordgren, J., Plogmann, S. & Neumann, M. (2001). *Phys. Rev. B*, **63**, 235117.
- Yamamoto, S., Senba, Y., Tanaka, T., Ohashi, H., Hirono, T., Kimura, H., Fujisawa, M., Miyawaki, J., Harasawa, A., Seike, T., Takahashi, S., Nariyama, N., Matsushita, T., Takeuchi, M., Ohata, T., Furukawa, Y., Takeshita, K., Goto, S., Harada, Y., Shin, S., Kitamura, H., Kakizaki, A., Oshima, M. & Matsuda, I. (2014). *J. Synchrotron Rad.* **21**, 352–365.